Identification of Tropical Cyclone Centers in SAR Imagery based on Template Matching and Particle Swarm Optimization Algorithms

Shaohui Jin[1], Xiaofeng Li[2], Xiaofeng Yang[3], Jun A. Zhang[4] and Donglang Shen[5]

[1]School of Information Engineering, Zhengzhou University, Zhengzhou, He'nan Province 450001, China

[2]GST at NOAA/NESDIS, College Park, MD, USA

[3]State Key Laboratory of Remote Sensing Science, Institute of Remote Sensing and Digital Earth, Chinese Academy of Sciences, Beijing 100101, China

[4] Hurricane Research Division at NOAA/AOML, and University of Miami/CIMAS, USA

[5] College of Marine Sciences, Shanghai Ocean University, Shanghai 201319, China, and also with the School of Coastal and Marine Systems Science, Coastal Carolina University, Conway, SC 29526 USA

For publication in

IEEE Transactions on Geoscience and Remote Sensing

Abstract

Synthetic Aperture Radar (SAR) has emerged as a new tool for tropical cyclone (TC) monitoring by providing information on the location of TC centers. However, SAR does not usually cover the entire TC domain due to its limited swath width. In this study, we develop a procedure to identify the location of the center of a TC when a SAR image only covers the rainband portion of the TC but not the eye. The algorithm is based on both an image processing procedure and the available knowledge of the inherent rainband structure of a TC. The three-step algorithm includes: (1) applying a Canny edge detector to find the curves associated with rainbands; (2) defining two filter criteria to select the spiral curves that resemble the estimation based on a TC rainband model; and (3) searching for the optimal matching solution using the Particle Swarm Optimization Algorithm (PSOA). Numerical experiments with images without TC eye information show that the proposed method can effectively locate the centers of TCs. We compare the experiment results with the Best Track Data to indicate the accuracy. Then we compare inflow angle model and the logarithmic spiral model, and find that the inflow angle model is more accurate for TC center identification.

Key words: Synthetic aperture radar, storms, pattern matching, filtering

1. Introduction

A tropical cyclone (TC) is a severe weather system that can lead to the loss of life and cause economic loss in coastal areas. TC tracking and intensity forecasting are the main tasks of operational meteorological agencies worldwide. Among the many TC parameters, the TC center location provides key information in monitoring and forecasting a TC's path and intensity. The accurate identification of a TC center location in real time will help TC forecasting.

Synthetic aperture radar (SAR), an active microwave sensor, has emerged as a new tool for TC monitoring and forecasting in recent years due to the increasing number SAR satellites in orbit. SAR radar pulses can penetrate through clouds and images the footprint of a TC with high spatial resolution (1 to 100 m) under all-weather conditions, day and night [1-3]. In addition, the sea surface roughness imaged by SAR can be inverted to sea surface wind, wave, and rain fields using existing geophysical model functions in both co- and cross-polarization configurations [4-8]. With the increasing number of available SAR satellites, especially the most recent Sentinel-1A [9, 10] and -1B [11], SAR imagery has drawn increasing attention as an emerging tool for monitoring and forecasting TCs.

TC eye extraction from SAR imagery is an important research topic. In the literature, Du and Vachon proposed a wavelet analysis method to extract TC eye shape in SAR images [12]. Recently, Jin *et al.* [13] developed algorithms based on a labeled watershed segmentation method and morphological analysis to extract hurricane eyes in SAR images. Lee et al. [14] extracted hurricane eyes from C-band SAR data based on a mathematical morphology method and discrete skeleton evolution. The two studies both compared their automatic TC eye extraction results with the manually extracted tropical cyclone morphology results from 85 SAR images systematically analyzed by Li *et al.* [1]. All the studies illustrate the potential of SAR in TC monitoring, but they targeted SAR imagery containing the entire TC system with obvious complete eyes. Although most well-developed TCs have complete eyes, other TCs at the developing or declining stages often do not have obvious eye structure. Moreover, SAR, due to its limited coverage, sometimes only covers part of a TC eye. Locating the centers of these types of TCs has not been fully addressed in the literature.

Traditionally, weather forecasters manually track the center and the rainbands of TCs using a time series of visible and IR satellite images. Sometimes, forecasters overlay a spiral template on a satellite image to find the best matching pattern so that they can determine the center of a TC by calculating the center of the best matched standard logarithmic spiral [15]. However, the center location results determined by these manual methods are subject to human errors.

In contrast to manual approaches, automatic methods can objectively locate a TC center on a SAR image costing less time. Numerical models usually use the lowest pressure to locate the TC center automatically, which need a sequence of images. Pattern matching method is another kind of methods which only need a single image. Wang et al. (2006) developed an auto-location of the center of a developing tropical cyclone based on image segmentation, mathematical morphology and Hough transform algorithm [16]. Wong and Yip (2008) proposed a method to fix the eye of a TC using a genetic algorithm with radar reflectivity data and temporal information [17-18]. Xu et al. (2009) proposed a spiral rainbands segmentation method by transforming it to a problem of classification using a support vector machine [19]. To our knowledge, no study has focused on using the pattern matching method to locate a TC center on a SAR image that does not contain a TC eye.

Recently, Jin et al. (2017) proposed a salient region detection and pattern matching-based algorithm for center detection of a partially covered tropical cyclone in a SAR image [20]. It is a semi-automatic center location method for partially covered TCs in SAR images. Rainbands of a TC are extracted using a salient region detection algorithm. Then the skeleton lines of rainbands are extracted using mathematical morphology. At last the PSOA and the inflow angle model are used estimate the TC center. Experiments demonstrate that this method can correctly locate a TC center in a SAR image with good accuracy. It extracts rainbands based on the saliency of TC structure on a TC SAR image and works well for most images. But there are several parameters need adjusted to extract rainbands correctly. Then rainbands are selected and skeleton lines are extracted by adjusting a few parameters. The artificial tuning will increase subsequently center location errors. Weather forecasts call for a more rapid method with less probability of error.

Based on this analysis, in this study we propose an automatic TC center location method that can be summarized as a three-step scheme: (1) apply a Canny edge detection algorithm to find the rainband curves in a SAR image; (2) define two filter criteria based on the length of each rainband curve and the ratio between the distance from the head to the end points and the length of each curve. The two filter criteria are used to select the spiral curves that resemble the results estimated from a published TC rainband model; and (3) transform the pattern matching problem into an optimization problem. A search for the optimal TC center solution is made by using the particle swarm optimization algorithm (PSOA).

The remainder of this paper is as follows: in Section 2, we introduce the algorithm. In Section 3, we apply the algorithm to three Envisat SAR images and two Radarsat-1 SAR images and one Sentine-1 SAR image to extract the TC center positions and compare our results with the logarithmic spiral model results. The discussions and conclusions are given in Section 4.

2. Locating the Center of TCs without Eyes based on PSOA

Generally speaking, TCs can be divided into TCs with eyes and TCs without eyes. In SAR images, a TC with eye appears as a dark eye area surrounded by bright and dark spiral rainbands system. A TC eye, with obvious dark features, has several shapes, such as circular eye, concentric double circular eye, elliptical eye, half circular ring eye, irregular eye, broken eye, etc. Rainbands can be classified into spiral rainbands, asymmetric rainbands and quasi-circular rainbands. Rainbands are the main structure we can use for extracting centers of TCs without eyes in SAR images.

Sometimes, a SAR image only covers part of a TC. This paper focused on developing a methodology to identify the TC center when a SAR image only covers the rainband portion of a TC. Another type of SAR image contains the TC eye but the eye structure is obscured. A TC tends to change its intensity when its eye becomes obscured. So, extracting the actual eye center in these situations is important.

A. Pattern Matching Models

Our automatic location of the center of a TC method adopts the pattern matching approach. With the help of a hurricane inflow angle model [21], and information extracted from the image (spiral curves) can be used to derive the actual TC center.

Here we choose an analytical near-surface (10 m) inflow angle model as a template to represent the TC surface wind structure to estimate the TC center. Because of the characteristic cyclonic flow near the sea surface in TCs, the documentation of observed surface wind directions is typically described in terms of surface inflow angles (α), which can be defined as the arctangent of the ratio of the radial to the tangential wind component (α = arctan (v_r/v_t)). Zhang and Uhlhorn [21] proposed a parametric model of inflow angle based on the analysis of near-surface inflow angles using wind observation data from over 1600 quality-controlled global positioning system dropwindsondes deployed by aircraft on 187 flights into 18 hurricanes. Analysis results indicate a statistically significant dependence of inflow angle on the radial distance from the TC center. The parametric model of inflow angle α in a TC can be provided by four parameters: the normalized radial distances (r^*), the azimuth angle measured clockwise from storm motion direction (θ), the maximum wind speed (V_{max}), and the storm motion speed (V_s). Of note, the maximum wind speed and the radius of V_{max} are determined using the SAR derived wind speed, and V_s is determined based on the best track data.

The inflow angle is defined as:

$$\alpha_{SR}(r^*,\theta,V_{\max},V_s) = A_{\alpha 0}(r^*,V_{\max}) + A_{\alpha 1}(r^*,V_s,V_{\max}) \times \cos\left[\theta - P_{\alpha 1}(r^*,V_s)\right] + \varepsilon \qquad (1)$$

where ε is the model error. $R^* = r/R_{max}$, where r is the radial distance measured in a polar coordinate system, and R_{max} is the radius of maximum wind speed. $A_{\alpha 0}$, $A_{\alpha 1}$, and $P_{\alpha 1}$ are defined as:

$$A_{\alpha 0} = a_{A0} r^* + b_{A0} V_{\max} + c_{A0} \qquad (2)$$

$$A_{\alpha 1} = -A_{\alpha 0}(a_{A1} r^* + b_{A1} V_s + c_{A1}) \qquad (3)$$

$$P_{\alpha 1} = a_{P1} r^* + b_{P1} V_s + c_{P1} \qquad (4)$$

The coefficients (*a,b,c*) are shown in Table 1. As an example, Fig.1 shows the horizontal map of the surface inflow angle from Hurricane Earl (2010). The inflow angle was calculated using Eq. (1) along with parameters based on the SAR image taken on September 2 (Table 2). It is evident from Fig. 1 that the inflow angle is asymmetrically distributed with the largest values being located at the front-right quadrant.

If we get a curve in a TC image, we can obtain all the pixels' positions on the curve. The distance r_i of one pixel (x_i,y_i) to the center (x_c,y_c) can be defined as:

$$r_i = \sqrt{(\mathrm{x}_i - \mathrm{x}_c)^2 + (\mathrm{y}_i - y_c)^2} \qquad (5)$$

The normalized distance r^*_i can be defined as:

$$r^*_i = \frac{\sqrt{(\mathrm{x}_i - \mathrm{x}_c)^2 + (\mathrm{y}_i - y_c)^2}}{\sqrt{(\mathrm{x}_{\max} - \mathrm{x}_c)^2 + (\mathrm{y}_{\max} - y_c)^2}} \qquad (6)$$

where (x_{max},y_{max}) is the position of the maximal wind speed. The corresponding azimuth can be defined as:

$$\theta_i = \arctan(\frac{y_i - y_c}{x_i - x_c}) \qquad (7)$$

r^* and θ can be determined if the center (x_c,y_c) of a TC and the position of the maximum wind speed are known. Therefore, the key to solving the matching problem is to find the best combination of parameters (x_c,y_c) that makes the inflow angles calculated from Eq. 1 best match those pixels on the rainband spiral curve. We can then transform the matching problem into an optimization problem. The optimum solution corresponds with the best match.

Another pattern matching model is the logarithmic spiral model. It was used in some literatures [16-18]. It can be defined as follows [26]:

$$\rho = ae^{b\theta} \tag{8}$$

In a rectangular coordinate system, it can be formulated as:

$$\begin{cases} x = \rho\cos\theta = ae^{b\theta}\cos\theta \\ y = \rho\sin\theta = ae^{b\theta}\sin\theta \end{cases} \tag{9}$$

The distance ρ_i of one point (x_i,y_i) on the spiral line to the center (x_c,y_c) and the corresponding included angle θ_i can be defined in Eqs. (5) and (7), respectively. If the center of a logarithm spiral is known, we can get parameters ρ and θ from Eqs. (5) and (7). If some points, (x_i,y_i) or (x_j,y_j) have been obtained, a and b in Eqs. (8) and (9) can be defined:

$$b = \frac{\ln\rho_i - \ln\rho_j}{\theta_i - \theta_j} \tag{10}$$

$$a = \frac{\rho_i}{e^{b\theta_i}} \tag{11}$$

As a result, a logarithm spiral can be determined by two parameters (x_c,y_c) if some points on the curve have been obtained. Our aim is to find a logarithm spiral that best matches with the spiral pattern of rainbands. We use the PSOA to search the best matched logarithm spiral. The fitness function in Step 2 is modified to:

$$z = \sum_{i=1}^{N}\sqrt{(\mathrm{x}_i - \mathrm{x}_c - \mathrm{ae}^{b\theta}\cos\theta)^2 + (\mathrm{y}_i - y_c - \mathrm{ae}^{b\theta}\sin\theta)^2} \tag{12}$$

The three-step proposed framework is shown in Fig. 2.

B. Spiral Curves Extraction using an Edge Detection Algorithm

Rainbands usually have obvious geometrical spiral characteristics. The spiral information is an important feature that can be used for locating the center of a TC that does not have an obvious eye feature. Therefore, it is necessary to extract useful spiral lines without the interference of unrelated features for automatic center location with pattern matching methods.

As a preprocessing procedure, we denoise the speckle noise in a SAR image. Speckle noise reduces the actual resolution of the SAR image, affects target identification and even causes some features to disappear in the image. A good de-noising algorithm should meet the following four criteria [22]: (1) remove the speckle noise effectively in the homogenous regions; (2) retain the edge and texture features as far as possible; (3) do not produce the pseudo Gibbs effect; and (4) maintain the radiation characteristics of radar images. Here we apply an extension of a non-local mean filter, the Probabilistic Patch-Based filter (PPB filter) that meets all 4 criteria to filter the speckle noise in SAR images [23]. The PPB filter is designed to smooth speckle noise in the homogeneous regions while preserving the edges and shapes at the same time. It is considered to be one of the best SAR image denoising methods. After denoising, the TC SAR images can be processed with little influence from speckle noise.

When locating the center of TCs, image segmentation using pattern matching is the common extraction method for spiral curve extraction [16]-[19]. Rainbands are first segmented with image segmentation methods, i.e., threshold segmentation method. Then morphological methods such as corrosion and expansion are used to eliminate hollows and protrusions in the connected regions to ensure that the skeleton lines extracted in the next step are as smooth as possible. However, it is difficult to use a simple threshold segmentation method to accurately extract rainbands. Complex image segmentation algorithms such as the segmentation of typhoon spiral cloud bands based on the support vector machine greatly increase the computational cost [19]. Besides, several times of corrosion and expansion which are two basic mathematical morphology operators operated on images will change the shape of rainbands. These processes will likely make the spiral curves obtained incomplete or inaccurate. Sometimes weather forecasters will draw along the trend of some rainbands manually when they need to extract spiral curves. This spiral curve edge detection algorithm greatly simplifies the operation steps and reduces the computational cost.

We find that the Canny algorithm, a classical edge detection algorithm, is valid in locating rainband edges on a SAR image [24]. At first, a TC SAR image is filtered by a two-dimensional Gaussian function so that its noise is reduced. Then, the amplitude and direction of the gradient image is calculated with a first order differential operator. Error detected edges are deleted by the non-maximum suppression of gradient amplitude. At last, edges from the candidate edge points are detected and connected with a double threshold.

In practical applications, affected by uneven illumination distribution or other factors, some TC SAR images may contain dark lines whose gradient characteristics are very similar to those of rainband edges. This will cause some meaningless edges in the final detected edge map. Generally, the gradient amplitudes of these dark lines are low, so we can set a small threshold when edges from the candidate edge points are detected and connected to label points whose gradient amplitudes are smaller than the threshold as non-edge points. This will avoid the contamination of dark lines.

C. Spiral Curves Selection with Two Filter Criteria

The edges of rainbands can effectively represent the spiral shape. However, not all edges found by the edge detector represent the rainband spiral shape. A number of detected edges are either too short or too irregular to represent the spiral shape. Therefore, it is necessary to select useful edges that contain spiral information before the pattern matching in the next step.

We choose two filter criteria to select spiral curves. Firstly, we calculate and rank the lengths of all the extracted edges, and only keep a few longest ones. Secondly, we calculate the distance between the head and tail points of each remaining edge, and then calculate the ratio between the curve length and the distance between the head and the end points. If the ratio is too small, the curvature of the edge curve is small and not in spiral shape. If the ratio is too large, the curve may contain too many irregular shapes for pattern matching. Therefore, we set two thresholds T1 and T2 to keep only spiral-shape edges whose ratios are in between. In our experiments the two thresholds are set as the ratios between the arc and the distance from one end point to the other end point of the arc when the radians are $\frac{\pi}{6}$ and $\frac{3\pi}{2}$, respectively.

D. Center Location of TCs based on PSOA

Given a spiral curve of a rainband obtained by the above two procedures, we can obtain all the pixels $\{(x_i, y_i)|(x_i, y_i) \in l_{ske}\}$ on it. As described previously, we need to find the best estimated center (x_{cbest},y_{cbest}) which makes the estimated inflow angles of pixels on the spiral curve closest to the actual inflow angles. So the key to solving the matching problem is to find the best combination of parameters (x_c,y_c). We take the matching problem as an optimization problem. The optimum solution corresponds to the best match.

In the literature, the Hough transform [16] is usually used as a simple and easy pattern matching method. However, it performs well on only a portion of the matching pixels, not all the matching pixels. It is also difficult to reach a good matching result across the entire image due to its limitations, such as complex calculation and poor detection performance when there is noise in an image. Wong et al. [18] used a genetic algorithm to match skeleton lines with a logarithm spiral model. The genetic algorithm is robust and has global search ability. However, crossover and mutation operators of the genetic algorithm guide the search iterative process randomly. So they provide the opportunity to evolve but inevitably produce the possibility of degradation at the same time. There will be a lot of redundant iterations when the solution reaches a certain range, resulting in the low efficiency of exact solutions.

The Particle Swarm Optimization algorithm (PSOA) is a method for optimization of continuous nonlinear functions [25]. It is simple and effective with fewer parameters than the genetic algorithm. The calculation quickly converges to the optimal solution. These advantages make PSOA widely used in solving optimization problems. In this study, we choose the PSOA to search the optimum solution to solve the matching problem.

The PSOA is based on research around birds' predation [25]. Researchers have found that the behavior of a flock of birds in flight is not predictable, and they will often suddenly change direction, spread, and so on. However, the whole flock always keeps consistency and they will keep the appropriate distance among birds. Based on the research on the behavior of such groups, researchers found that there is a kind of social information sharing mechanism which provides an advantage for the evolution of the group. This is the basis of the formation of the PSOA. Suppose there is a group of birds looking for food randomly. Every bird can be seen as a solution in the PSOA' solution space, which is also called a particle. If there is only one piece of food, the easiest but most effective strategy for finding the food is to search the surrounding area of the bird that is nearest to the food. Each bird adjusts its flight direction and speed according to its own flight experience and other birds' flight experience. The best position for a bird in flight is the best solution for the bird itself, which can be called pbest. The best position of the whole group is the best solution to the whole group, which can be called gbest. There is a fitness value z determined by an optimization function. Every bird follows the current optimum particle to search for its best position in the solution space. If a better solution is found, the current optimum bird's position and speed are replaced. The process repeats until the optimum solution is reached.

Combined with the binary image of skeleton lines of rainbands, the PSOA is used to find the best center (x_{cbest},y_{cbest}) from which we can obtain the inflow angles that are closest to the given model inflow angles. In the experiments, a binary image of spiral curves is input. We count the number of curves and get all the pixel positions of each spiral curve. As shown in Fig. 3, the following three steps are operated for each skeleton line:

Step 1: Initialize the position and speed of the original searching particle (pixel samples on a skeleton line). The original position of each particle can be considered as its original pbest. Calculate the corresponding fitness value of each particle. The best fitness value is considered as the global fitness value. The position of the particle having the best fitness value can be considered as the original gbest.

A matching result can be evaluated by the deviations of the given inflow angle and the corresponding evaluated inflow angle. The smaller the deviation is, the better the overlapping is. So the fitness function is defined as:

$$z = \sum_{i=1}^{N} \left| \alpha_{SR_i} - \{A_{\alpha 0}(r^*_i, V_{\max}) + A_{\alpha 1}(r^*_i, V_s) \times \cos\left[\theta_i - P_{\alpha 1}(r^*_i, V_s)\right] + \varepsilon\} \right| \quad (13)$$

Step 2: Calculate the fitness value of each particle. If the fitness value of one particle is better than the current pbest, update the current pbest. If the best pbest of all particles is better than the current gbest, update the current gbest. The speed and position of each particle can then be changed following formula (14) and formula (15):

$$v_{i+1} = w \cdot v_i + c1 \cdot r1 \cdot (pbest_i - present_i) + c2 \cdot r2 \cdot (gbest_i - present_i) \quad (14)$$

$$present_{i+1} = present_i + v_{i+1} \quad (15)$$

Where c1 and c2 are acceleration coefficients, and r1 and r2 are random numbers between 0 and 1.

Step 3: If the iterative time has reached the preset maximum number or the result has reached the minimum error, iteration stops and the optimum solution is provided. Otherwise, go to step 2.

The optimum solution of (x_c,y_c) from PSOA calculation is considered as the estimated center of the TC. Sometimes there may be several spiral lines after skeleton lines extraction. Each spiral line has an optimal solution. Theoretically, there is a center point which is the compromise optimal solution for all the spiral lines. So we take the average of all the optimum as the final center point.

3. Experimental Results

The data used in this paper are three Envisat TC SAR images, two Radarsat-1 TC SAR images, and one Sentine-1 TC SAR images (Fig. 4). The Envisat SAR images were acquired in wide swath mode (WSM) with a medium resolution of 150 m and a swath of 405 km. The Radarsat-1 SAR images are ScanSAR wide beam (SCW) images with a medium resolution of 100 m and a swath of 500 km. The Sentine-1 SAR image is an Extra Wide Swath (EW) image with a resolution of 20 m × 40 m. Detailed information about these images is given in Table 2. The images of TC Talim and TC Earl contain a complete TC structure. The images of TC Gustav and TC Gaston contain the TC eye and a part of the rainband. These images originally contained entire eyes. To demonstrate the effectiveness of our algorithm, we purposely removed the eye regions before applying the algorithm. The image of TC Franklin contained a fuzzy eye area, and the image of TC Karl contained no eye.

Figs. 5(a)–10(a) show the denoised SAR images of TCs. As shown in these figures, the PPB filter can effectively restrain speckle noise and preserve the texture and the edge information at the same time, being conducive to the following edge extraction. Figs. 5(b)–10(b) show the edge maps after Canny edge detection. Each edge map contains edges of the general outline of a TC and some local spiral curves. However, the edge maps also contain edges of irrelevant patterns and some small disconnected edge lines. As shown in Fig. 11, some of these edge lines are too straight, too short, or too complicated in shape. These edges do not reflect the spiral shape and rotation characteristics of TCs. We selected these edges useful for extracting spiral shapes following the two filter criteria described in Section 2.2. Here the two thresholds are the ratios between the arc and the distance from one end point to the other end point of the arc when the radians are $\frac{\pi}{6}$ and $\frac{3\pi}{2}$, respectively. Figs. 5(c)–10(c) show the selected edge maps. It can be seen that the remaining curves after selection contain spiral information and are long enough for pattern matching in the following procedure.

With the selected spiral curves, we transform the matching problem into an optimization problem and use the PSOA to search the optimal solution. Each optimum solution corresponds to an estimated center of the TC. If there are several spiral curves in a selected edge curves map at the same time, we will get several optimum solutions for one TC image. The center points obtained after matching have deviations, so the TC center can be considered as the mean of these points. The parameters in our experiments are set as follows: $c_1 = c_2 = 2$ and $r_1 = r_2 = 1$, and the maximum velocity of particles is 5. The population size is set to 20 and the evolution time is set to 200. The red points in Figs. 5(d)–10(d) are the final obtained center of the TC. Here we didn't discuss the eccentricity of the TC eye. We suppose that the TC center is within the eye area. It can be seen from Figs. 5(d)–8(d) that the TC center matches the real TC eye. The TC eye in Fig. 9(d) is within the fuzzy eye area.

To evaluate the accuracy of our center location results, we compare the estimated center with the NOAA Best Track Data sets in Table 3 and Fig. 12. The NOAA Best Track Data is obtained from NOAA's program "International Best Track Archive for Climate Stewardship (IBTrACS)". It is updated every 6 hours, which contain the center position (usually it is the latitude and longitude) and the intensity (described by the maximum wind speed or the lowest central air pressure) of a TC at a certain time and other information. The locations of the TC centers in the SAR imaging times are interpolated from the two nearby Best Track data records. The estimated center position of a TC should be between the center positions at the two recorded times. Table 3 shows each estimated center's position and the two center positions on the two above recorded times in the best track data set. Using linear interpolation, we draw a straight line between the center positions before and after the time that each

SAR image was captured. Then we point out the estimated center position in the same figure. Theoretically the estimated center position should be on the line. We can see in Fig. 12 that the estimated centers of TCs Talim, Gustav, and Gaston are almost on the straight lines, and those of TCs Earl and Karl are close to the straight lines. However, the estimated center position of TC Franklin is far away from its straight line, and its longitude and latitude are a little out of the range. These samples illustrate that our method is effective and accurate in most cases.

We then provide a comparison between the logarithmic spiral model and the inflow angle model. A set of estimated TC centers in a SAR image obtained with the inflow angle model and the logarithm spiral model is shown in Table 4. We can see that the centers estimated with the inflow angle model are relatively close to each other. The biggest distance from one estimated center to the average center is no more than 5 pixels. However, the centers estimated with the logarithm spiral model are discrete, and the biggest distance from one estimated center to the average center can be more than 50 pixels. Although the final average result is more or less the same, some estimated points obtained with the logarithm spiral model are outliers. While the volute tendency of the rainbands appears spiral, the shapes are various, and not all the rainbands conform to the volute tendency of the logarithmic spiral. So matching the rainbands with the logarithmic spiral model is limited, and the matching performs well for some but not all TCs. The inflow angle model is more robust and accurate than the logarithm spiral model. One issue with the inflow angle model is that we need to know the actual inflow angles of required points of a TC and its maximum wind speed when we apply the model. However, the results show that we can also use the average inflow angle when the inflow angles of each point are unknown. This can also achieve accurate results, although the results may be not as accurate as the results obtained with the actual inflow angles of each point.

4. Conclusions

The automatic location of the center of TCs, especially the automatic location of TCs without eyes, is an important task in typhoon monitoring. Based on the characteristics of TCs in SAR images, we propose a method based on rainband pattern matching and the PSOA to automatically locate center of a TC without an eye in a SAR image. We show experiment samples containing three Envisat TC SAR images, two Radarsat-1 TC SAR images, and one Sentinel-1 TC SAR image to validate our method. These samples contain two kinds of TCs: a SAR image showing the complete structure of a TC and a SAR image showing part of a TC. The experimental results show the accuracy of our method. We then compare the inflow angle model with the logarithm spiral model and experimental results show that the inflow angle model is more robust and accurate than the logarithm spiral model.

The method in reference [20] proposed a complex visual saliency method containing several steps to obtain the curves suitable for pattern matching. These steps all need adjusted parameters. The method needs a large amount of calculation and is time-consuming. Different from the salient region detection method [17], the edge detection method in this paper greatly simplifies the calculation for obtaining the spiral line with fewer parameters. This will reduce the error and greatly improve the computational efficiency. A Canny detector is a classical algorithm, which is easy to operate with fewer parameters. The inflow angle model is proposed based on the analysis of observational data. It is suitable for many TCs but not all TCs. In addition, the initialization of particles and the change strategy of particle positions of the PSOA will both affect the optimization results. This makes the experiment results more or less depending on subjective experience. It is an issue to find a more effective method and to select curve lines of rainbands in a future work.

Acknowledgments

The SAR images were provided by the European Space Agency under project 141 and 6133. The views, opinions, and findings contained in this report are those of the authors and should not be construed as an official NOAA or U.S. Government position, policy, or decision.

References

[1] X. F. Li, J. A. Zhang, X. F. Yang, W. G. Pichel, M. D. Maria, D. Long, and Z. W. Li, “Tropical cyclone morphology from spaceborne synthetic aperture radar,” *Bull. Amer. Meteorol. Soc.*, vol. 94, pp. 215-230, 2013.

[2] G. Zheng, J. Yang, A. K. Liu, X. Li, W. G. Pichel, and S. He, “Comparison of typhoon centers from SAR and IR images and those from best track datasets,” *IEEE Trans. Geosci. Remote Sens.*, vol. 54(2), pp. 1000-1012, 2016.

[3] K. Friedman and X. Li, “Storm patterns over the ocean with wide swath SAR,” *J. Hopkins APL Tech. D.*, vol. 21(1), pp. 80-85, 2000.

[4] G. S. Zhang, W. Perrie, X. Li, and J. A. Zhang, “A Hurricane morphology and surface wind vector estimation model for C-band cross-polarization SAR,” *IEEE Trans. Geosci. Remote Sens.*, 2017.

[5] P. Hwang, X. Li, and B. Zhang, “Retrieving hurricane wind speed from dominant wave parameters,” *IEEE J. Sel. Topics Appl. Earth Observ. Remote Sens.*, 2017.

[6] G. S. Zhang, X. Li, W. Perrie, B. Zhang, and L. Wang, “Rain effects on the hurricane observations over the ocean by C-band Synthetic Aperture Radar,” *J. Geophys. Res. Oceans*, vol. 120, 2015.

[7] F. Xu, X. Li, P. Wang, J, Yang, W. Pichel, and Y-Q Jin, “A backscattering model of rainfall over rough sea surface for synthetic aperture radar,” *IEEE Trans. Geosci. Remote Sens.*, 2015.

[8] A. A. Mouche, B. Chapron, B. Zhang and R. Husson, “Combined Co- and Cross-Polarized SAR Measurements Under Extreme Wind Conditions”, IEEE Trans. Geosci. Remote Sens., vol. 55(12), pp.1-10, 2017.

[9] X. F. Li, “The First Sentinel-1 SAR Image of a Typhoon,” *Acta Oceanol. Sin.*, vol. 34(1), pp. 1–2, 2015.

[10] A. A. Mouche, B. Chapron, B. Zhang and R. Husson, “Combined Co- and Cross-Polarized SAR Measurements Under Extreme Wind Conditions”, IEEE Trans. Geosci. Remote Sens., vol. 55(12), pp.1-10, 2017.

[11] L. Q. Huang, B. Liu, X. F. Li, Z. H. Zhang and W. X. Yu, “Technical Evaluation of Sentinel-1 IW Mode Cross-Pol Radar Backscattering from the Ocean Surface in Moderate Wind Condition”, Remote Sens. , vol. 9(8),:854, 2017.

[12] Y. Du and P. W. Vachon, “Characterization of hurricane eyes in RADARSAT-1 images with wavelet analysis,” *Can. J. Remote Sens.*, vol. 29, pp. 491-498, 2003.

[13] S. H. Jin, S. Wang, and X. F. Li, “Typhoon eye extraction with an automatic SAR image segmentation method,” *Int. J Remote Sens.*, vol. 35, pp. 3978-3993, 2014.

[14] I. Lee, A. Shamsoddini, X. Li, J. C. Trinder, and Z. Li, “Extracting hurricane eye morphology from spaceborne SAR images using morphological analysis,” *ISPRS J. Photogramm. Remote Sens.*, vol.. 7, pp. 115-125, 2016.

[15] M. V. Sivaramakrishnan and M. Selvam, “On the use of the spiral overlay technique for estimating the center positions of tropical cyclones from satellite photographs taken over the Indian region,” *In Proceedings of the 12th conference on radar meteorology*, pp. 440–446, 1996.

[16] P. Wang, C. S. Guo, Y. X. Luo, “Local spiral curves simulating based on Hough transformation and center auto-locating of developing typhoon,” *Trans. Tianjin Univ.*, vol. 12, pp. 142-146, 2006.

[17] K. Y. Wong and C. L. Yip, "Tropical cyclone eye fix using genetic algorithm with temporal information," *Knowledge-Based Intelligent Information and Engineering Systems*, vol. 3681, pp. 854-860, 2005.

[18] K. Y. Wong, C. L. Yip, and L. P. Wah, "Automatic tropical cyclone eye fix using genetic algorithm," *Expert Syst. Appl.*, vol. 34, pp. 643-656, 2008.

[19] J. W. Xu, P. Wang, and Y. Y. Xie, "Image segmentation of typhoon spiral cloud bands based on support vector machine," *ICML*, vol. 2, pp. 1088-1093, 2009.

[20] S. H. Jin, S. Wang, X. F. Li, L. C. Jiao, J. A. Zhang, and D. L. Shen, "A salient region detection and pattern matching-based algorithm for center detection of partially covered tropical cyclone in a SAR image," *IEEE Trans. Geosci. Remote Sens*, vol. 55(1), pp. 280-291, 2017.

[21] J. A. Zhang and E. W. Uhlhorn, "Hurricane sea surface inflow angle and an observation-based parametric model," *Am Meteorol Soc.*, vol. 140, pp. 3587-3605, 2012.

[22] C. Oliver and S. Quegan, "Understanding Synthetic Aperture Radar images," Boston MA：Artech House, pp. 158-187, 1998.

[23] C. A. Deledalle, L. Denis, and F. Tupin, "Iterative weighted maximum likelihood denoising with probabilistic patch-based weights," *IEEE T Image Process*, vol. 18, pp. 2661-2672, 2009.

[24] J. Canny, "A computational approach to edge detection," *IEEE Trans. Pattern Anal. Mach. Intell.*, vol. 8(6), pp. 679-698, 1986.

[25] R. Eberhart and J. Kennedy, "A new optimizer using particle swarm theory," *The 6th Int. Symposium on Micro Machine and Human Science*, Nagoya, pp. 39-43, 1995.

[26] C. Baumgarten and G. Farin, "Approximation of logarithmic spirals," *Comput. Aided Geom. Des.*, vol. 14(6), pp. 515-532, 1997.

Table 1. Coefficients for the inflow angle model.

Equation	Variables	a	b	c
(2)	$A_{\alpha 0}$	-0.90	-0.90	-14.33
(3)	$A_{\alpha 1}$	0.04	0.05	0.14
(4)	$P_{\alpha 1}$	6.88	-9.60	85.31

Table 2. Detailed information about TC SAR images.

TC	Time	Satellite	Polarization	Band	Mode	Resolution
Talim	2005.08.30	Envisat	VV	C	WSM	150
Earl	2010.09.02	Envisat	VV	C	WSM	150
Gustar	2008.09.01	Envisat	VV	C	WSM	150
Gaston	2016.08.30	Sentine-1	VV	C	EW	20
Franklin	2005.07.28	Radarsat-1	HH	C	SCW	100
Karl	2004.09.20	Radarsat-1	HH	C	SCW	100

Table 3. Estimated centers with our method and centers from the best track data set records before and after the time that SAR images are captured.

Tropical Cyclone	UTC Time	Estimated Center (Lat, Lon)	UTC Time Before	Best Track Center (Lat, Lon)	UTC Time After	Best Track Center (Lat, Lon)
Talim	2005.08.30 01:24:30	(21.5,129.3)	2005.08.30 00:00:00	(21.4,129.7)	2005.08.30 06:00:00	(21.7,128.5)
Earl	2010.09.02 15:01:25	(30.9,-74.9)	2010.09.02 12:00:00	(30.1,-74.8)	2010.09.02 18:00:00	(31.7,-75.1)
Gustav	2008.09.01 03:56:50	(27.4,-88.4)	2008.09.01 00:00:00	(26.9,-87.7)	2008.09.01 06:00:00	(27.9,-89.0)
Gaston	2016.08.30 14:45:12	(32.1,-53.2)	2016.08.30 12:00:00	(32,-53.5)	2016.08.30 18:00:00	(32.4,-52.5)
Franklin	2005.07.28 22:16:05	(38.0,-67.6)	2005.07.28 18:00:00	(37.1,-68.0)	2005.07.29 00:00:00	(38.4,-66.6)
Karl	2004.09.2 0 08:56:44	(17.0, -45.3)	2004.09.20 06:00:00	(17.0, -45.2)	2004.09.2 0 12:00:00	(17.5, -46.0)

Table 4. The set of TC centers estimated with the inflow angle model and the logarithm spiral model.

	Experiments with Inflow Angle Model		**Experiments with Logarithm Spiral Model**	
	$(x_c)_{best}$	$(y_c)_{best}$	$(x_c)_{best}$	$(y_c)_{best}$
	732.6795	600.0751	751.3455	576.6757
	730.6201	596.7512	722.5519	541.8418
	732.1334	599.7162	764.4380	571.6392
	729.3550	594.1986	710.3034	551.5651
	732.6288	599.7210	767.6173	559.4478
	733.4454	598.3882	775.5809	562.1592
	732.5794	600.4000	766.5757	579.7024
	733.8792	601.0111	771.7417	578.7290
	732.4486	598.8011	749.0303	571.4776
	732.3128	599.5379	782.2646	565.7211
average	732.2082	598.8600	756.1449	565.8959

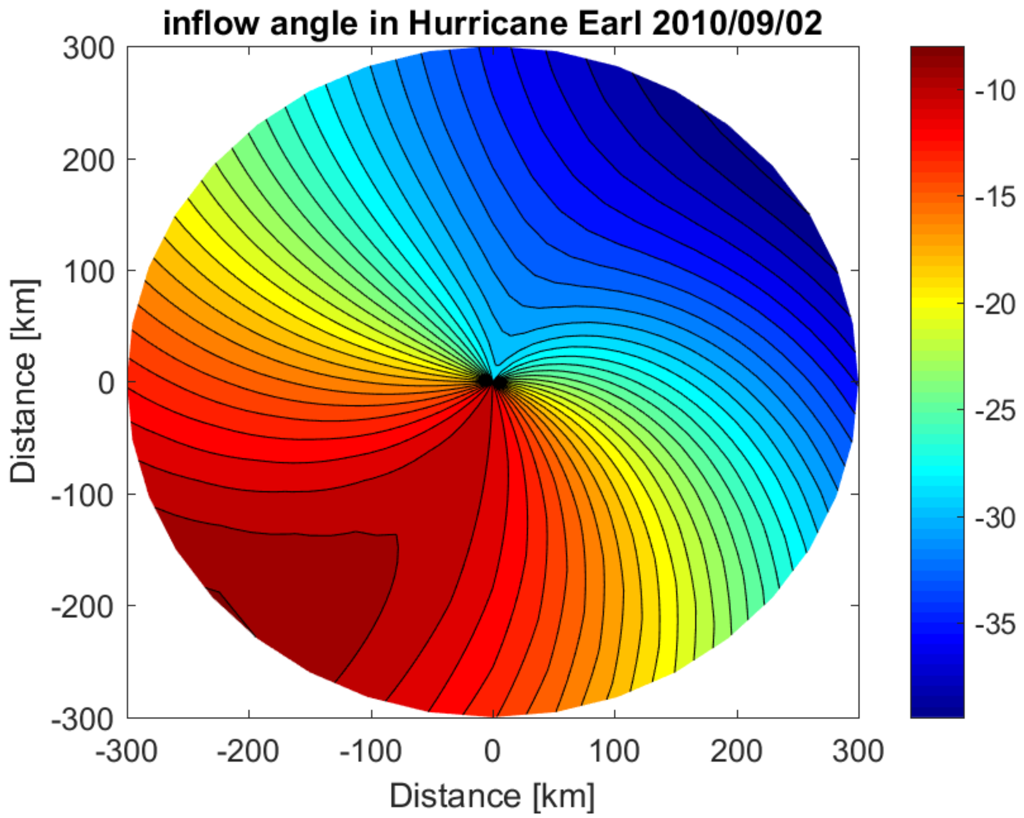

Fig. 1. 2D Plot of the surface inflow angle as a function of distance to the storm center based on information of the SAR image taken on September 2, 2010.

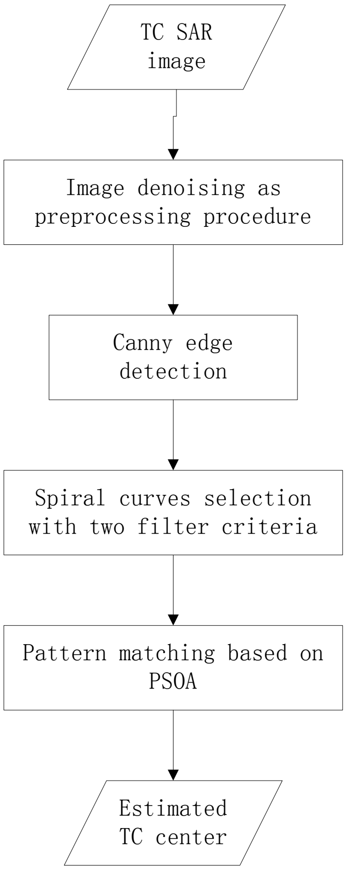

Fig. 2. The framework of center location of TCs without eyes with our method.

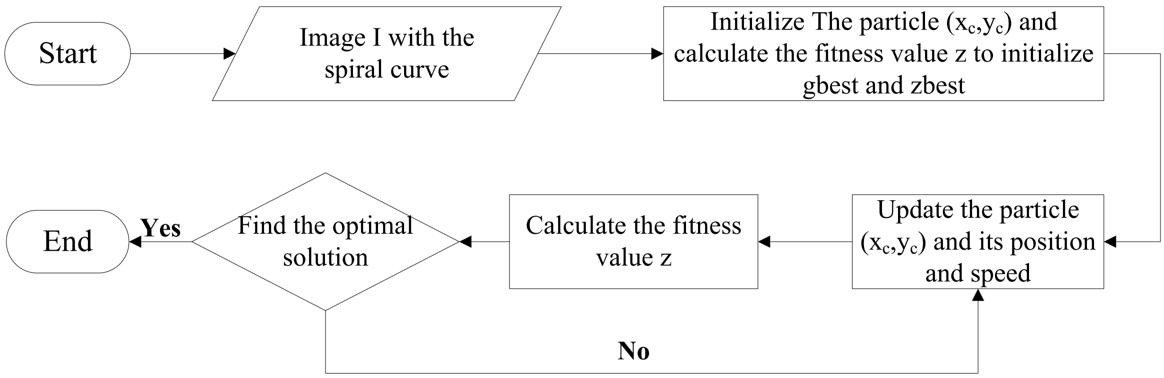

Fig. 3. Scheme of the PSOA.

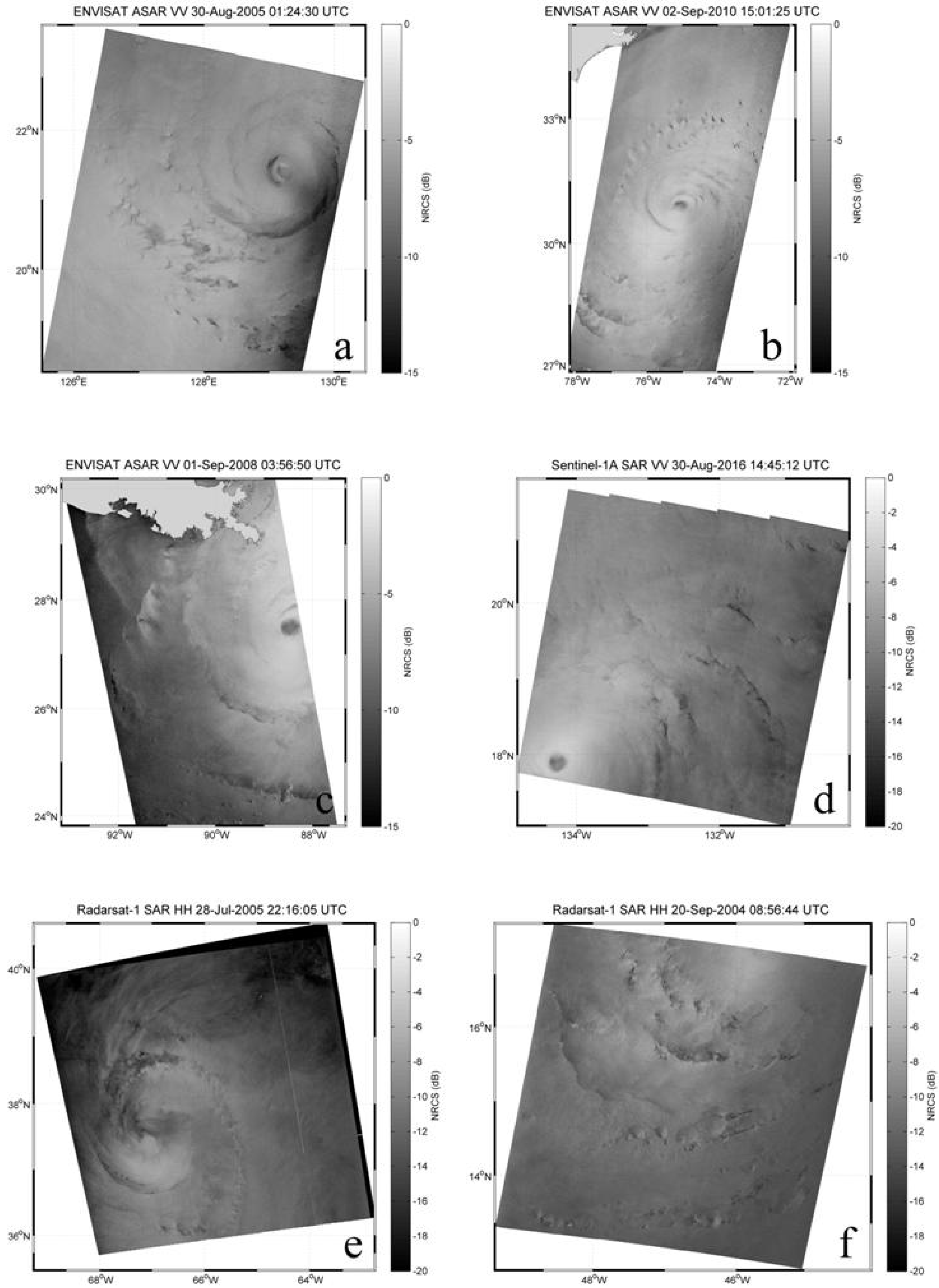

Fig. 4. The TCs shown in the paper and their geographical positions.

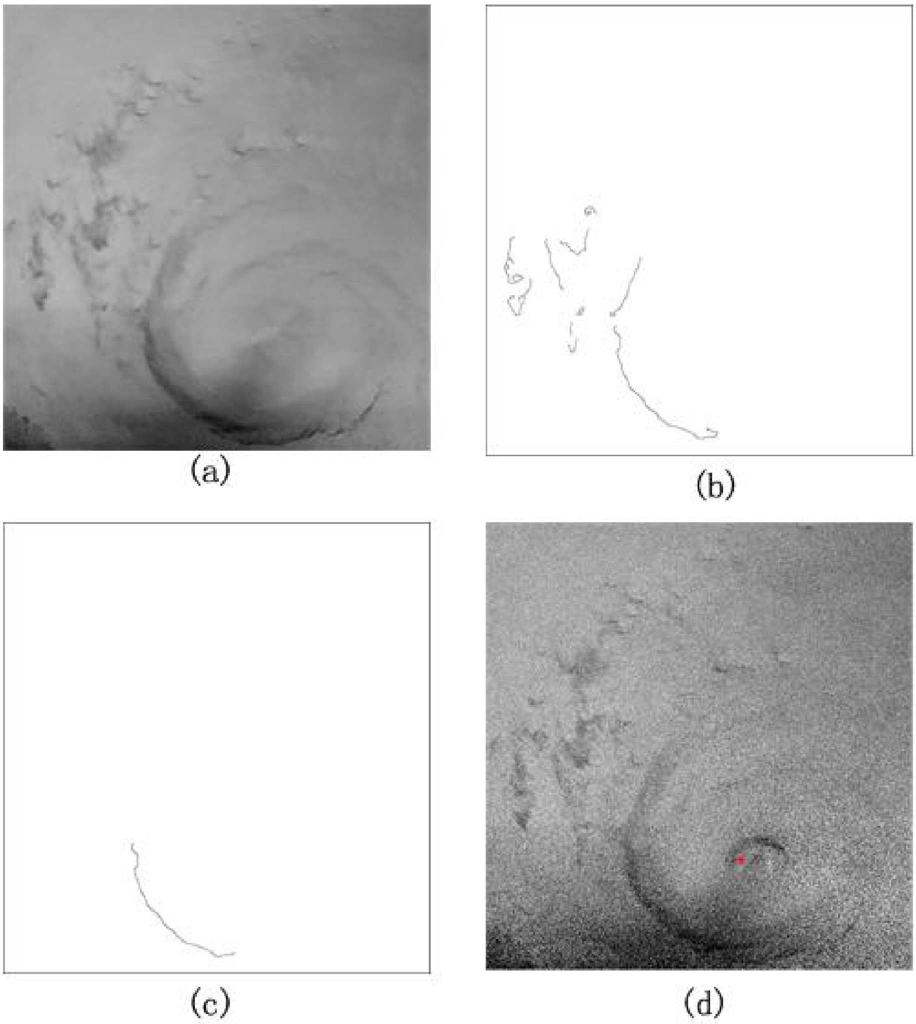

Fig. 5. The results for TC Talim. (a) The denoised SAR images of TC Talim without eye. (b) The edge maps after Canny edge detection. (c) The selected edge curves maps. (d) The estimated center of TC Talim shown on the original SAR image.

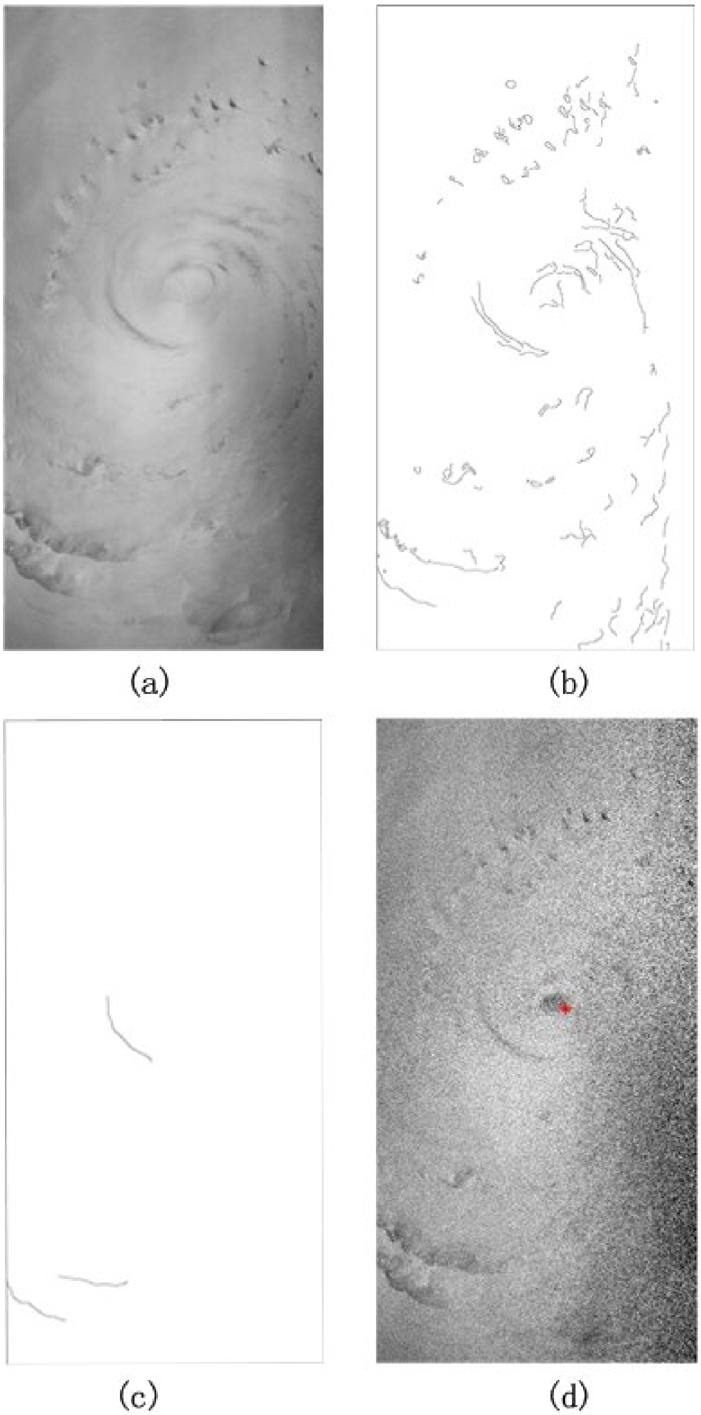

Fig. 6. The results for TC Earl. (a) The denoised SAR images of TC Earl without eye. (b) The edge maps after Canny edge detection. (c) The selected edge curves maps. (d) The estimated center of TC Earl shown on the original SAR image.

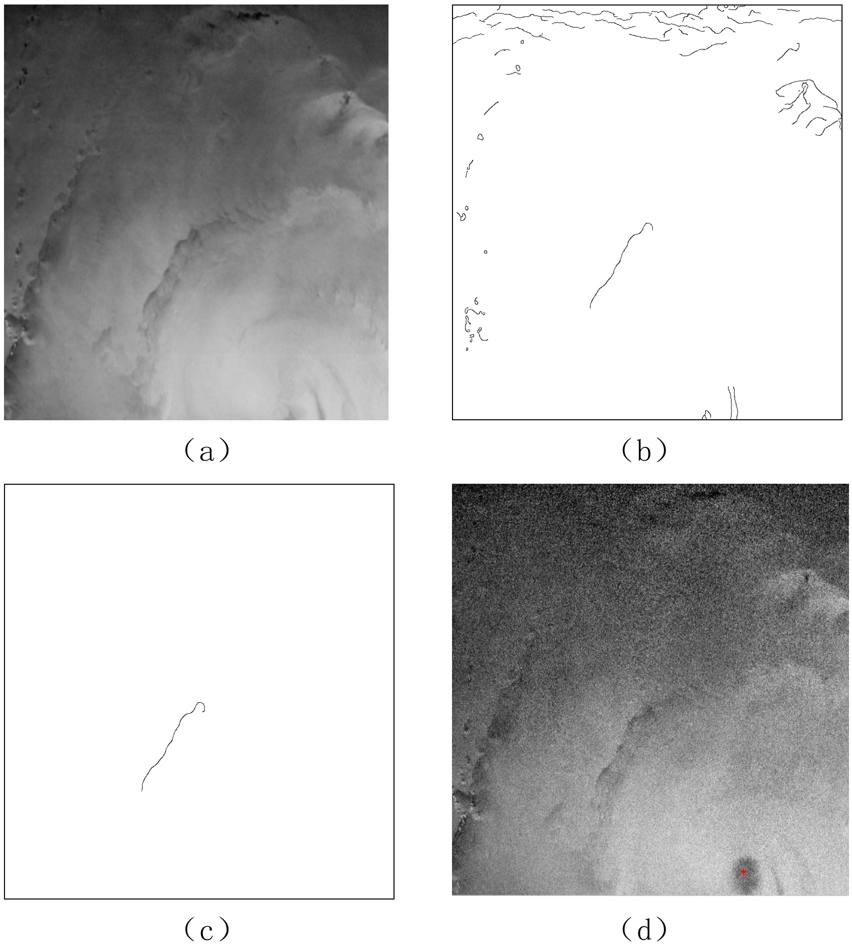

Fig. 7. The results for TC Gustav. (a) The denoised SAR images of TC Gustav without eye. (b) The edge maps after Canny edge detection. (c) The selected edge curves maps. (d) The estimated center of TC Gustav shown on the original SAR image.

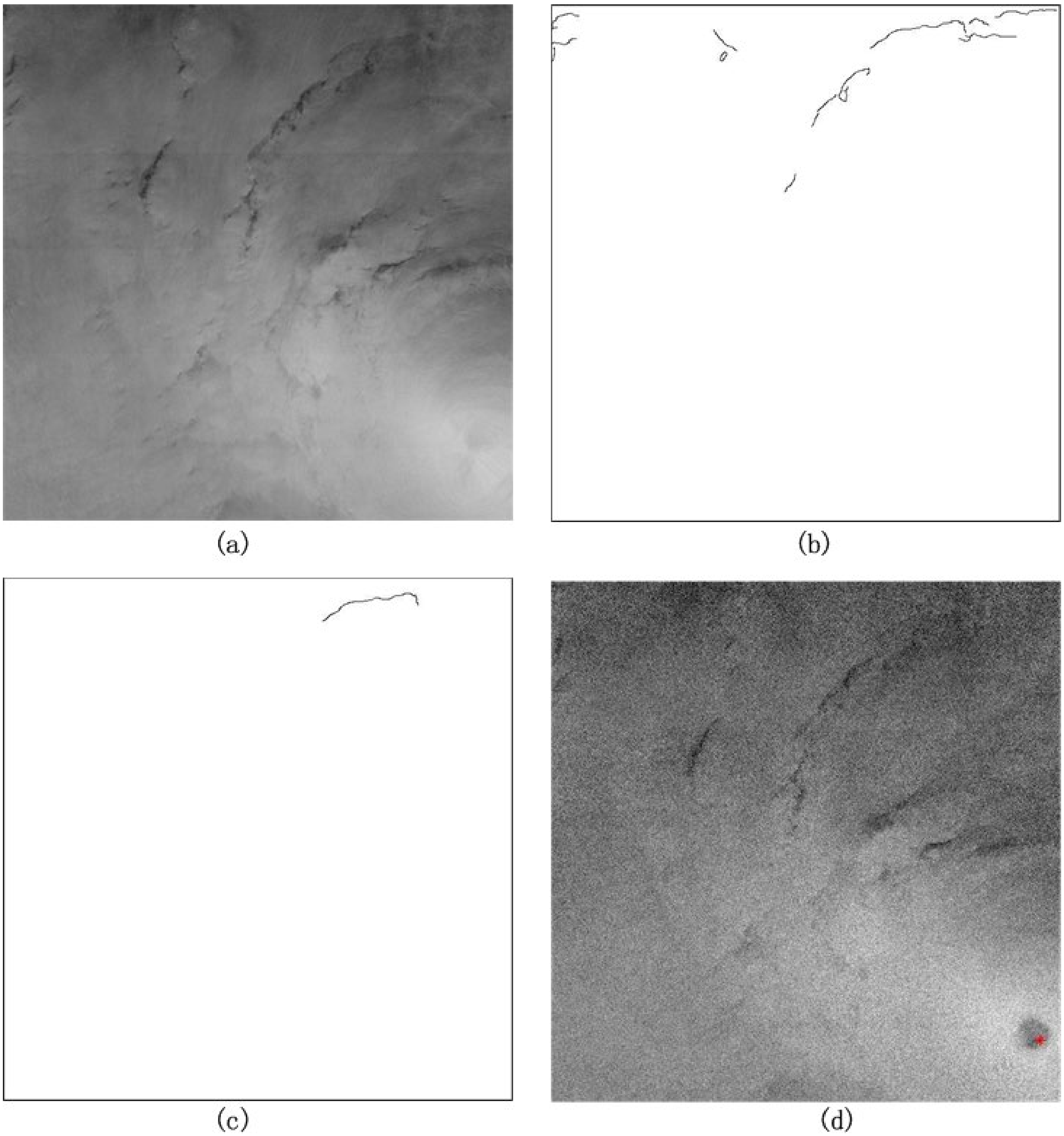

Fig. 8. The results for TC Gaston. (a) The denoised SAR images of TC Gaston. (b) The edge maps after Canny edge detection. (c) The selected edge curves maps. (d) The estimated center of TC Gaston shown on the original SAR image.

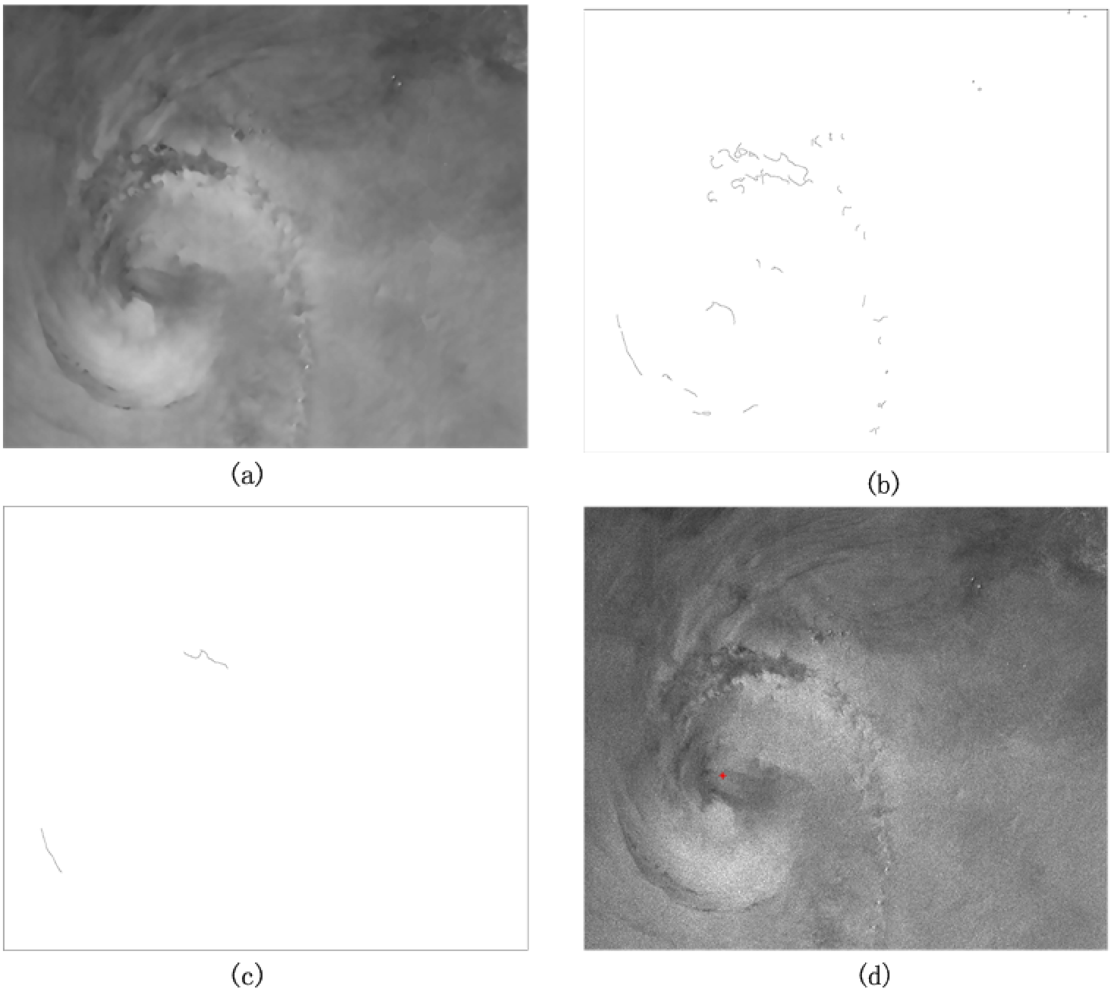

Fig. 9. The results for TC Franklin. (a) The denoised SAR images of TC Franklin. (b) The edge maps after Canny edge detection. (c) The selected edge curves maps. (d) The estimated center of TC Franklin shown on the original SAR image.

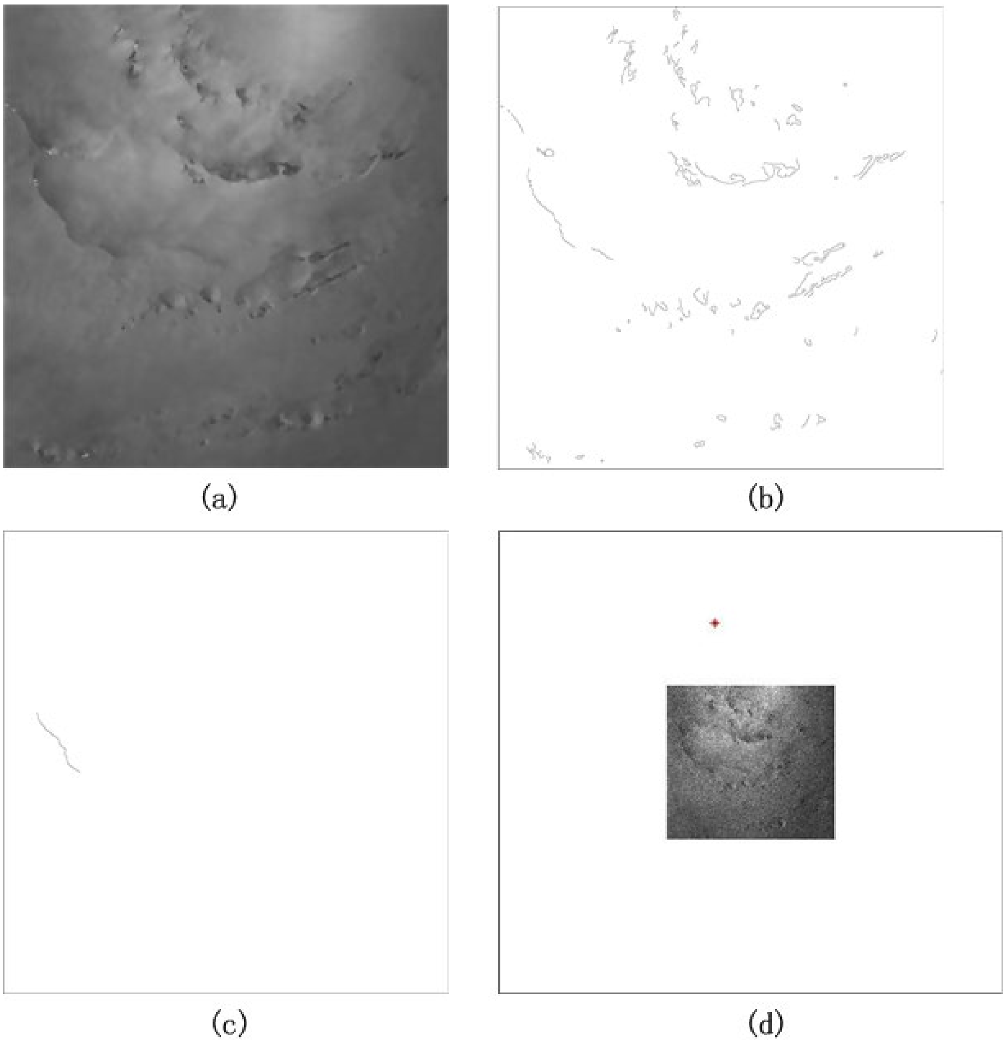

Fig. 10. The results for TC Karl. (a) The denoised SAR images of TC Karl. (b) The edge maps after Canny edge detection. (c) The selected edge curves maps. (d) The estimated center of TC Karl shown on the original SAR image.

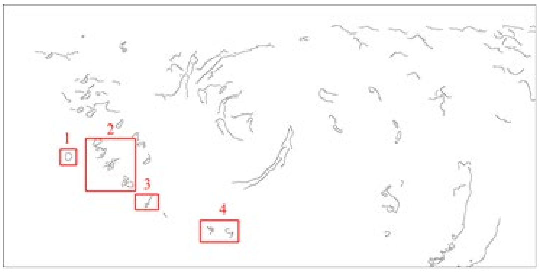

(a)

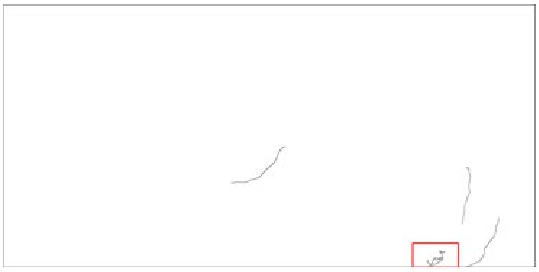

(b)

Fig. 11. Select curves which can be used for effective pattern matching. (a) In the red rectangle frames, some curves are too short, some look like straight lines, and some are complex. (b) In the red rectangle frame, after length selection, there are still curves whose shapes are complex. So we need select again.

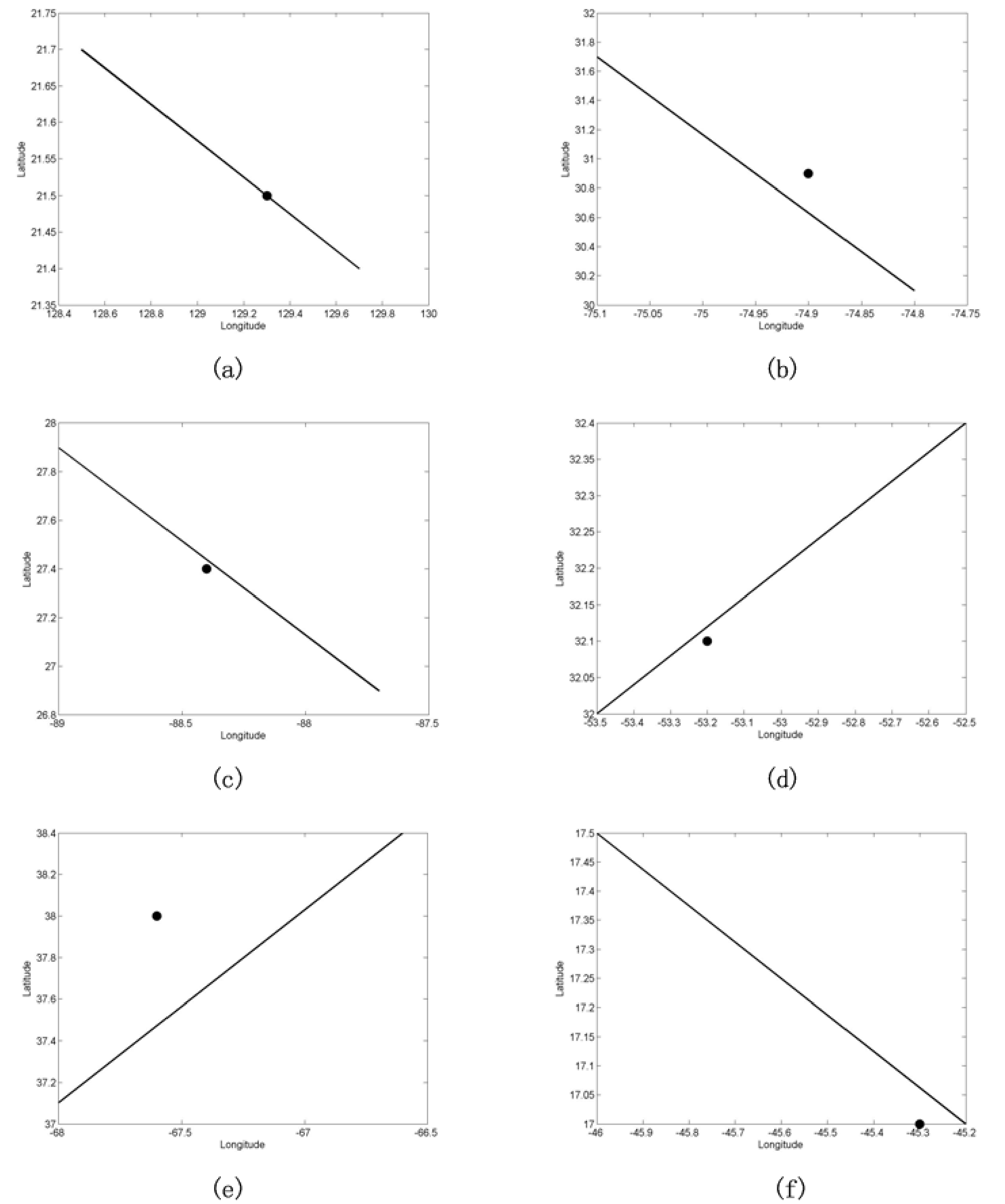

Fig. 12. The position of each estimated center and the straight line between the center positions in the best track data sets recorded before and after the time that the SAR images are captured. Fig.12.(a) –(f) corresponding to Fig.4.(a)-(f),respectively.